Journal of Theoretical and Applied Physics (JTAP), Special Issue: AICIS'23-Article 02

Proceeding of the 3rd Annual International Conference on Information and Sciences 2023, University of Fallujah, Iraq

https://dx.doi.org/10.57647/j.jtap.2024.si-AICIS23.02

Synthesis of two-phase TiO_2 nanoparticles via in-situ one-step process for photocatalytic applications

Rasha Jameel Neama*, Firas K. Mohamad Alosfur, Noor J. Ridha, Khawla J. Tahir, Rajaa A. Madlol

Department of Physics, College of Science, University of Kerbala, Kerbala, Iraq.

***Corresponding author:** rsha.j@s.uokerbala.edu.iq

Original Research

Published online: 15 June 2024

Abstract:

Titanium dioxide (TiO_2) nanoparticles (NPs) were synthesized by a simple sol-gel technique. The prepared sample was characterized by X-ray diffraction (XRD), X-ray photoelectron spectroscopy (XPS), transmission electron microscopy (TEM), field emission scanning electron microscopy (FESEM), and Brunauer–Emmett–Teller (BET). The results showed that the prepared TiO_2 NPs have agglomerated spherical shapes with anatase and rutile phases, TiO_2 consists of Ti 2p and O 1s regions. The average anatase and rutile TiO_2 crystallite size were estimated to be 32.38 nm and 37.37 nm, respectively. The BET result showed that TiO_2 had a surface area of 33.36 m_2 g^{-1}. Doses of different TiO_2 nanoparticles (5, 10, 15, 20, and 25 mg) were used to study the photocatalyst degradation of methylene blue (MB) under UV light. The dose of 15 mg was the optimal dose to degrade 68.39% of the dye within two hours.

Keywords: TiO_2; Sol-gel; XPS; Photocatalytic; Methylene blue

1. Introduction

Due to industrial advancement, the quantity of water pollution created by human activities has increased dramatically in recent decades. During the same historical, the need for clean water for human use such as industry and agriculture expanded dramatically [1]. While dyes are known as a source of water contamination, the textile industry continues to use dyes widely. Depending on how they are disposed of, dyes can pollute land and water when released. Therefore, it is crucial to treat these dye effluents to maintain clean, land, and water [2].

The photocatalytic process is the most efficient way to purify water since it is inexpensive and can be performed at atmospheric pressure and room temperature [3–5]. Many studies have found that titanium dioxide (TiO_2) is the best photocatalytic material for the degradation of an organic dye like MB, due to the electron-hole pair generated by light exposure's low rate of recombination. Irradiating TiO_2 nanoparticles with ultraviolet (UV) light wavelengths generates pairs of electrons and holes [6]. TiO_2 stands as a frequently employed photocatalyst material for the degradation of organic pollutants in water. This preference arises from its distinctive characteristics, including high photocatalytic activity, cost-effectiveness, chemical stability, and non-toxic nature [7]. In contrast, the morphology and crystalline structure of TiO_2 can significantly impact its photocatalyst efficiency [8–10].

TiO_2 presents in three crystalline phases: anatase, rutile, and brookite [11]. Each phase has different chemical and physical characteristics, resulting in different performances in devices made from them [12]. Many different synthesis methods have been employed to synthesize TiO_2, such as polyol solvothermal [13], hydrothermal [14], chemical vapor deposition (CVD) [15], microwave [16], electro-spinning [17], sol-gel [18] and others. Although all of these described technologies may produce significant quantities of nanomaterial, the sol-gel process is more common than the others [19–21], due to its simplest, economical, and most widely used way to produce TiO_2 nanoparticles. TiO_2 nanostructures can be prepared with different morphologies, such as nanorods [22], nanotubes [23], nanowires [24], nanobelts [25], nanospheres [26], hollow-sphere [27], and others. The morphologies and crystal structures of TiO_2 can be controlled by the synthesis conditions.

TiO_2 photocatalytic activity is typically determined by a variety of factors, including phase [28], surface area [29], minimum crystal size [30], and catalysis dose [31]. In this paper, TiO_2 nanoparticles were prepared via a sol-gel process. The photocatalytic performance of the prepared TiO_2 nanoparticles with different doses under UV irradiation was studied by the decomposition of an aqueous MB solution.

2. Experimental

2.1 Materials

All of the components used in the synthesis process were not purified. Titanium (IV) Isopropoxide (TTIP, $Ti(C_{12}H_{28}O_4)$, 97%) used as a TiO_2 precursor material and purchased from Sigma-Aldrich, pure ethanol (C_2H_6O, 99.9%), Hydrochloric Acid (HCl, $HClO_3$, 36.5 - 38.0%) were purchased from J. T. Baker and Deionized water (DI, H_2O, High degree of purity) to the preparation process of the product. A target pollutant in an aqueous solution was methylene blue (MB, $C_{16}H_{18}ClN_3S$, 99%).

2.2 Preparation of TiO_2 nanoparticles

First, 10 mL of TTIP was added dropwise to the beaker containing 50 mL of ethanol (EtOH) under vigorously stirred at 600 rpm for 10 minutes. After the titration process was completed, the solution's color changed from clear to milky white, suggesting the production of TiO_2 NPs. Next, a mixture of 50 mL ethanol, 10 mL H_2O, and 1 mL HCl was added dropwise to the solution under continued stirring for 30 min. The final solution will keep immobile for two nights until the formation of the gel.

Then the drying process takes place, where the sample is placed in the oven for about 60 hours at a temperature of 75 °C to get rid of unwanted materials. After this step, the powder was obtained by manually grinding the sample. Then the sample was annealed using an oven under an ambient atmosphere at 450 °C for 2 hours to improve the crystallinity. as shown in Fig. 1.

2.3 Characterization methods

A variety of methods were used to analyze the obtained sample, including X-ray diffraction (XRD) to examine the structure of the prepared powder and the recording of X-ray diffraction profiles analysis pattern using an X-ray Diffractometer Model-XRD Philips PW1730 with Cu Kα radiation for $\lambda = 0.15406$ nm. For a 2θ angle scanning range of 10 – 80°, step width of 0.02°, 40 mA, and X-ray operation of 40 KV, the diffraction data was acquired. The surface properties of the sample were characterized by using the XPS BESTEC EA10 spectrometer instrument. The spectra obtained were fitted by CASAXPS software (Casa XPS Version 2.3.16 PR 1.6) using a Shirley background. The TEM Philips EM 208S microscope observed the shape and particle size of the prepared sample. Further study about the sample morphology was achieved using FESEM with an operating voltage of about 20 kV and an image magnification is (35, 135) kx.

Finally, the surface area of the sample was calculated using the BET BELSORP Mini II device by subjecting it to N_2 adsorption at a temperature of 77 K.

2.4 Photocatalysis

Using UV light (Xenon lamp, 250 W, 365 nm wavelength) maintained at room temperature with a stationary evacuator to prevent any heat catalytic effect, the photocatalytic degradation of MB was studied. Various weights (5, 10, 15, 20, and 25 mg) of the generated catalyst were mixed

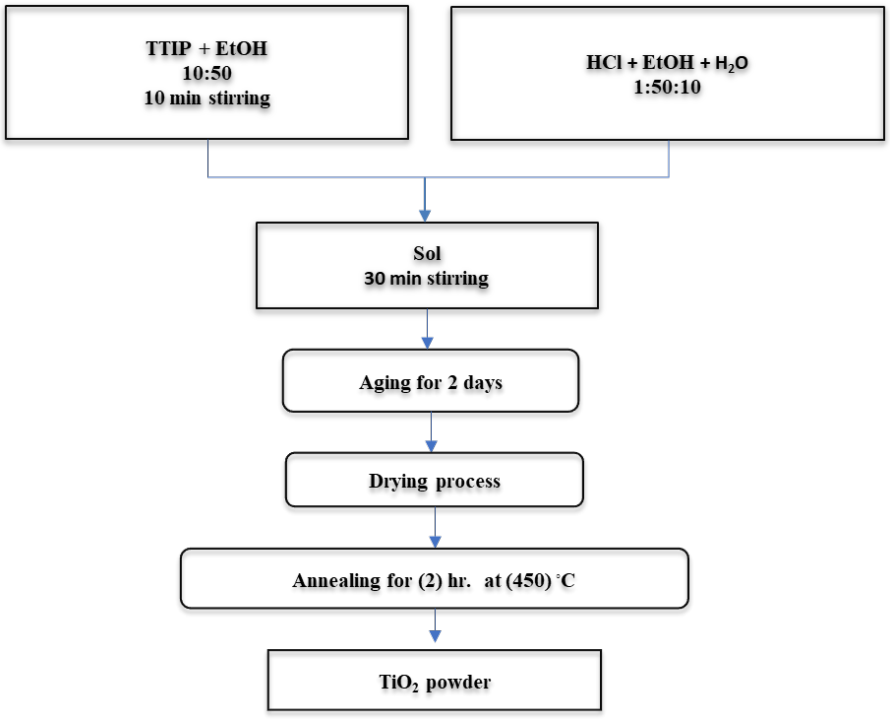

Figure 1. Flow chart of TiO_2 preparation using sol-gel.

for ten minutes in a beaker with 100 mL of MB at 10 ppm concentration. The mixture was then left in the dark for 30 minutes to establish adsorption and desorption equilibrium. The reacted materials were then subjected to UV radiation to evaluate photodegradation behavior. A specific amount (4 mL) of liquid was taken out every twenty minutes during the irradiation operations. Then the solutions were centrifuged for 10 minutes at 4000 rpm to remove the catalyst. These solutions of deterioration (K_{app}) and photodegradation efficiency (PDE), the formulas below applied [32]:

$$\ln \frac{C_0}{C_t} = K_{app} t \tag{1}$$

$$PDE = \frac{C_0 - C_t}{C_0} \times 100 \tag{2}$$

where C_0 and C_t are the MB concentrations before and after UV irradiation exposure respectively. C_t was calculated by drawing the calibration curve. Consequently, the apparent rate constant (K_{app}) may be determined by computing the slope of a plot of $\ln(C_0/C_t)$ vs. time (t) [33].

3. Results and discussion

3.1 XRD analysis

Figure 2 shows the XRD pattern of the prepared powder. X-ray diffraction pattern of TiO_2 NPs peaks is related to two phases (anatase and rutile mixed phase). The stronger peaks located at $2\theta = 27.76°, 36.33°, 39.48°, 41.46°, 44.45°, 56.89°, 64.29°, 69.70°$, and $70.03°$ correspond to the (110), (101), (200), (111), (210), (220), (310), (301) and (112) planes, respectively. The resulting peaks agreed well with the standard results data of the rutile phase (ICDD 01-088-1173 TiO_2). The peaks located at $2\theta = 25.54°, 38.14°, 48.30°, 54.59°, 63.13°$ and $75.13°$ responded to the (101), (112), (200), (211), (204) and (215) planes, correspondingly [34]. They are highly compatible with the standard results data of the anatase phase (ICDD 00- 002-0406 TiO_2) [35]. The stronger peak appeared in the XRD test agreeing with the (110) plane appearing at 27.76° of the diffraction patterns, indicating the formation of the TiO_2 tetragonal Rutile phase. The average crystallite size of anatase and rutile TiO_2 were estimated to be 32.38 nm and 37.37 nm, respectively by using the Scherrer equation for domain peak (110).

3.2 X-ray photoelectron spectroscopy (XPS) analysis

TiO_2 NPs survey XPS spectra for the whole binding energy area are shown in Fig. 3. The typical peaks of C 1s, O 1s, and Ti 2p were observed from the spectra. The photoelectron peaks were calibrated using the 284.8 eV value for the C 1s binding energy.

Usually, since carbon is typically present as adsorbed material on any XPS sample measured, it serves as a convenient reference [36]. The peak position of TiO_2 was located at 284.50 eV which in comparison with standard C 1s observed (~ -0.30 eV) deviation.

Figure 4 displays the Ti 2p region spectra of TiO_2 NPs. The appearance of the two major photoelectron peaks of TiO_2 NPs with binding energies of 458.20 and 464.05 eV, respectively, indicated Ti (IV) $2P_{3/2}$ and $2P_{1/2}$. The peak of Ti (IV) $2P_{3/2}$ at 458.20 eV is ascribed to the titanium metallic (Ti°) meanwhile the other peak Ti $2P_{1/2}$ at 464.05 eV [37]. There is a split orbital of about 5.85 eV due to the metallic state of TiO_2 representing the standard Ti^{4+} state of the anatase TiO_2 [38].

Figure 5 shows two peaks, one at 529.15 eV and the other at 530.19 eV, which can be seen in the O 1s characteristic of TiO_2 NPs. These peaks are ascribed to surface-adsorbed oxygenated species (OS) and lattice oxygen (LO), respectively [39].

Table 1 displays the outcomes of the XPS analysis conducted on the entirety of the sample after applying the deviation from the standard, encompassing both atomic ratios and the precise determination of peak positions.

3.3 TEM analysis

TEM images were utilized to demonstrate the shape, particle size, and particle size distribution of TiO_2 nanoparticles as

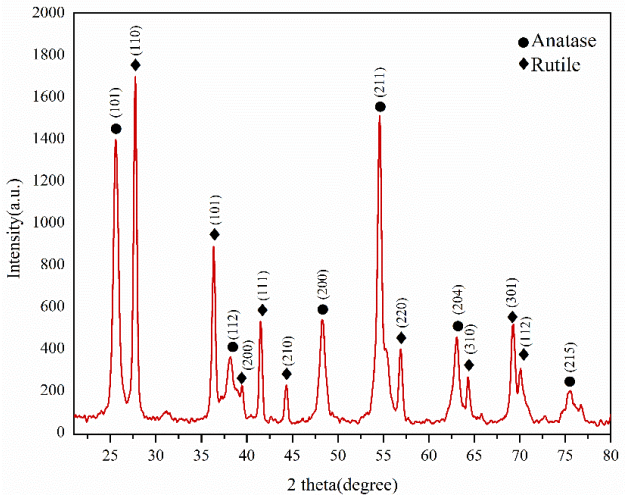

Figure 2. The produced powder's X-ray diffraction patterns of TiO_2.

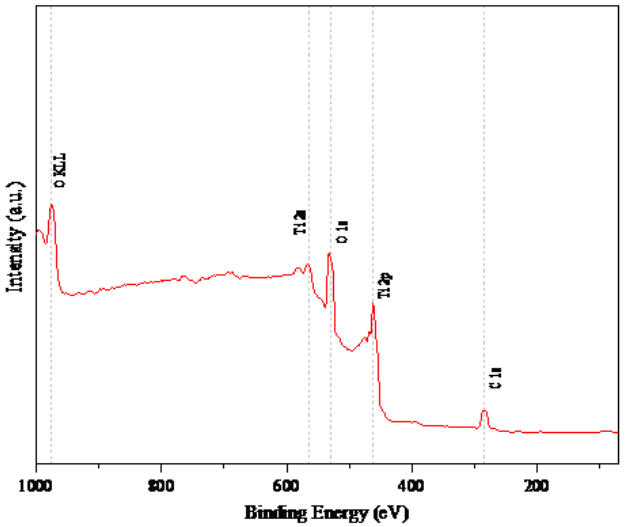

Figure 3. TiO_2 NPs surface survey XPS spectra.

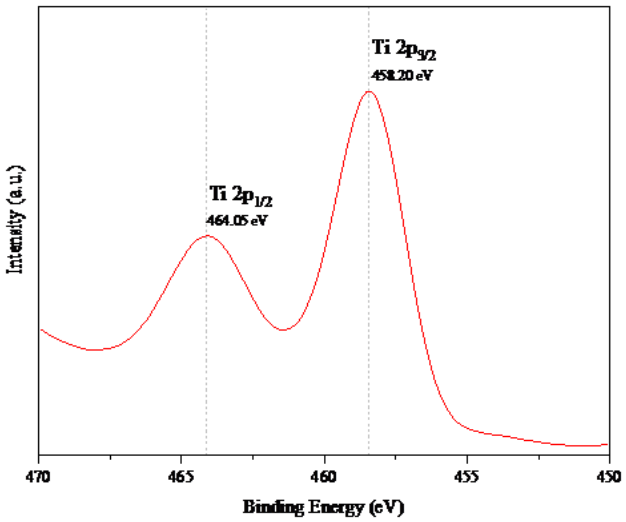

Figure 4. Ti 2p, XPS region spectra of TiO_2 NPs.

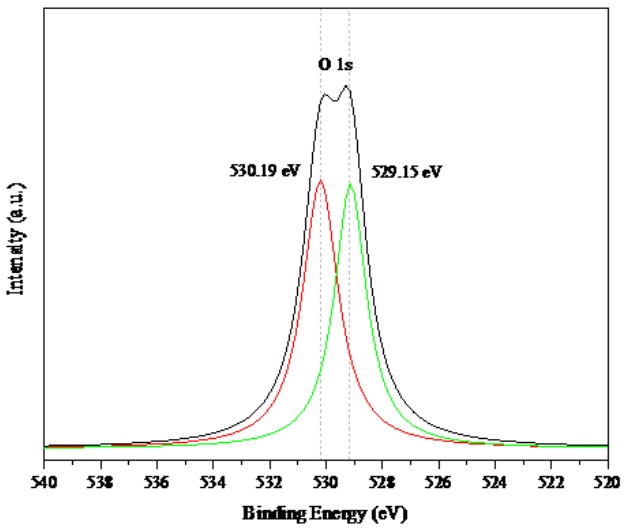

Figure 5. XPS region spectra of TiO_2 at O 1s.

shown in Fig. 6. Because of the aggregation of original particles consisting of either single particles or clusters of particles, the TiO_2 particles had an uneven shape. The average size and size distribution of nanoparticles were calculated from TEM pictures using Image tool software, with at least 100 particles from the sample considered. It is observed that the TiO_2 nanoparticles were spherical. The average particle size and the size range of the TiO_2 were ~ 31 nm.

3.4 FESEM analysis

The morphology of the prepared sample was investigated using FESEM as shown in Fig. 7. The results revealed that the structure of the prepared TiO_2 has agglomerated non-uniform spherical NPs with an average particle size of ~ 27.93 nm. The agglomeration occurs due to the TiO_2 being unstable in the nanoparticle form so they will tend to join each other until they are relatively stable. These results agreed well with previously published work [40].

3.5 BET analysis

The surface area of the photocatalyst sample is an important factor that affects dye degradation activity [41]. Fig. 8 depicts the N_2 adsorption-desorption curve of the produced TiO_2 NPs. The relative isotherms were a type IV isotherm with an H1 hysteresis loop [42], the adsorption and desorption isotherms of TiO_2 nanoparticles split into four zones. The isotherms showed a steady rise in adsorption in region i with a relative pressure (P/P_0) less than (0.3), indicating that the samples have micropores with a smaller size (2 nm). The relative pressure in region ii was between (0.3 and 0.8), and the isotherms displayed mild hysteresis loops, indicating that the samples include intermediate pores with sizes ranging from (2 nm to 30 nm) [43]. The isotherms demonstrate a distinctive capillary focus in region iii when the relative pressure is between (0.8 and 0.93) [44]. Capillary condensation became noticeable at elevated relative pressure (P/P_0), as indicated by the noticeable increment in adsorption volume observed in the upper segment of isotherms once the pores have become saturated with N_2-liquid [45]. Finally, a little hysteresis existed in region iv with a maximum relative pressure greater than (0.9) reflecting the fact that the pores were filled with N_2 gas. The computed BET surface area from the N_2 isotherm was 33.36 m^2g^{-1}. The cumulative pore size curve for the BJH desorption is represented in the inset figure in Fig. 8 and verifies the existence of uniform pores (10.25 nm).

3.6 MB degradation

According to extensive research, the amount of catalyst used in photocatalytic degradation plays a significant influence in the degradation of organic compounds or dyes. To achieve the maximum photocatalytic activity, the amount of catalyst must be optimized. The experiment was performed with different doses of TiO_2 (5, 10, 15, 20, and 25 mg), with an initial dye concentration of 10 ppm (10 mg/L), under UV-light irradiation for 2 hours. Fig. 9 shows the absorption spectra of MB under UV irradiation.

Table 1. Spectral features of TiO_2 NPs.

Element/Transition	Peak energy (eV)	Concentration (at. %)	Peak assignment
C	1s	284.80	adventitious carbon
O	1s	529.15	lattice oxygen in TiO_2
Ti	$2P_{3/2}$	458	Ti (IV) in TiO_2

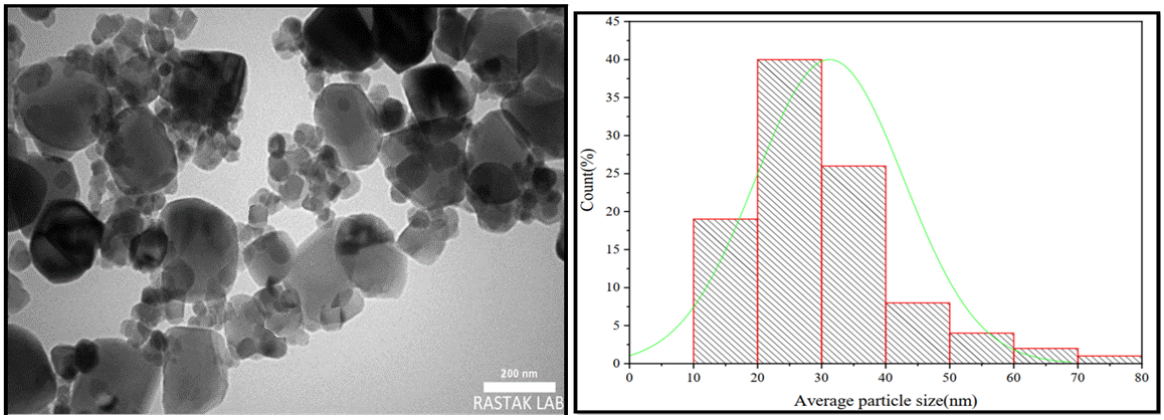

Figure 6. TEM images particle size and particle size distribution of TiO_2.

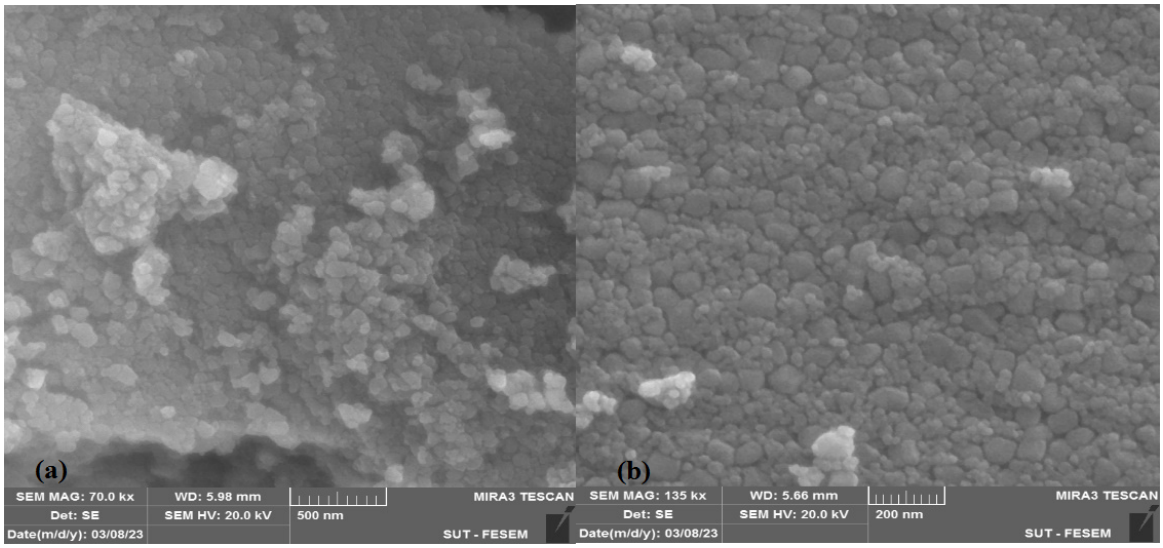

Figure 7. TiO_2 NPs FESEM micrographs, at various magnifications, including (a) 70 kx and (b) 135 kx.

Generally, it was observed that as the irradiation time increased, the intensities of the maximum absorption peaks decreased. Because of the tiny crystal size of the TiO_2, the absorption peaks of MB were slightly blue-shifted. This process is evident in the increase of electron and hole reduction and oxidizing potentials, respectively [46].

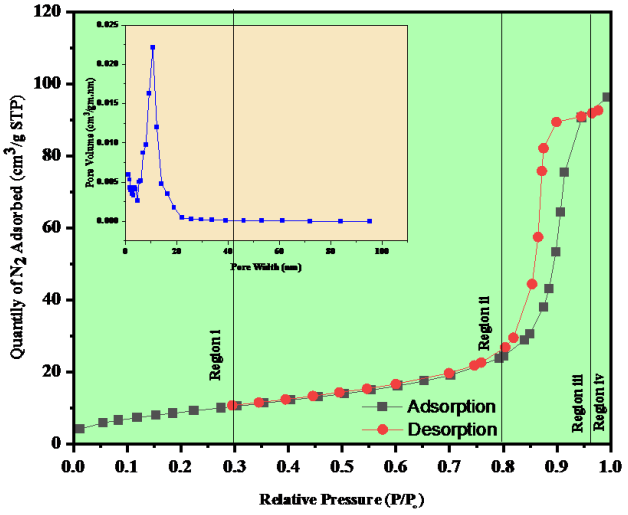

Figure 8. N_2 adsorption-desorption isotherm BET of TiO_2, the inset is average pore diameter TiO_2.

Figure 10 displays the C/C_0 concentration ratios of MB (at 664 nm) with the degradation time (t). The rate of decomposition raised with an increasing dose of catalyst and then decreased after a certain dose of catalyst. The catalyst dose of 15 mg TiO_2 showed the highest degradation efficiency of methylene blue under UV-light irradiation conditions. At 20 and 25 mg, the degradation efficiency of methylene blue was reduced due to a rise in solution opacity generated by increased doses of TiO_2 particles, which resulted in a decrease in light penetration. After 120 min of ultraviolet irradiation, the maximum removal performance of methylene blue with catalyst loading (15 mg) for a given time was 68.3%, indicating that the prepared TiO_2 showed significant photocatalytic activity. This is due to the strong reduction and oxidation power in electrons and holes which increased the rate of photodegradation [47].

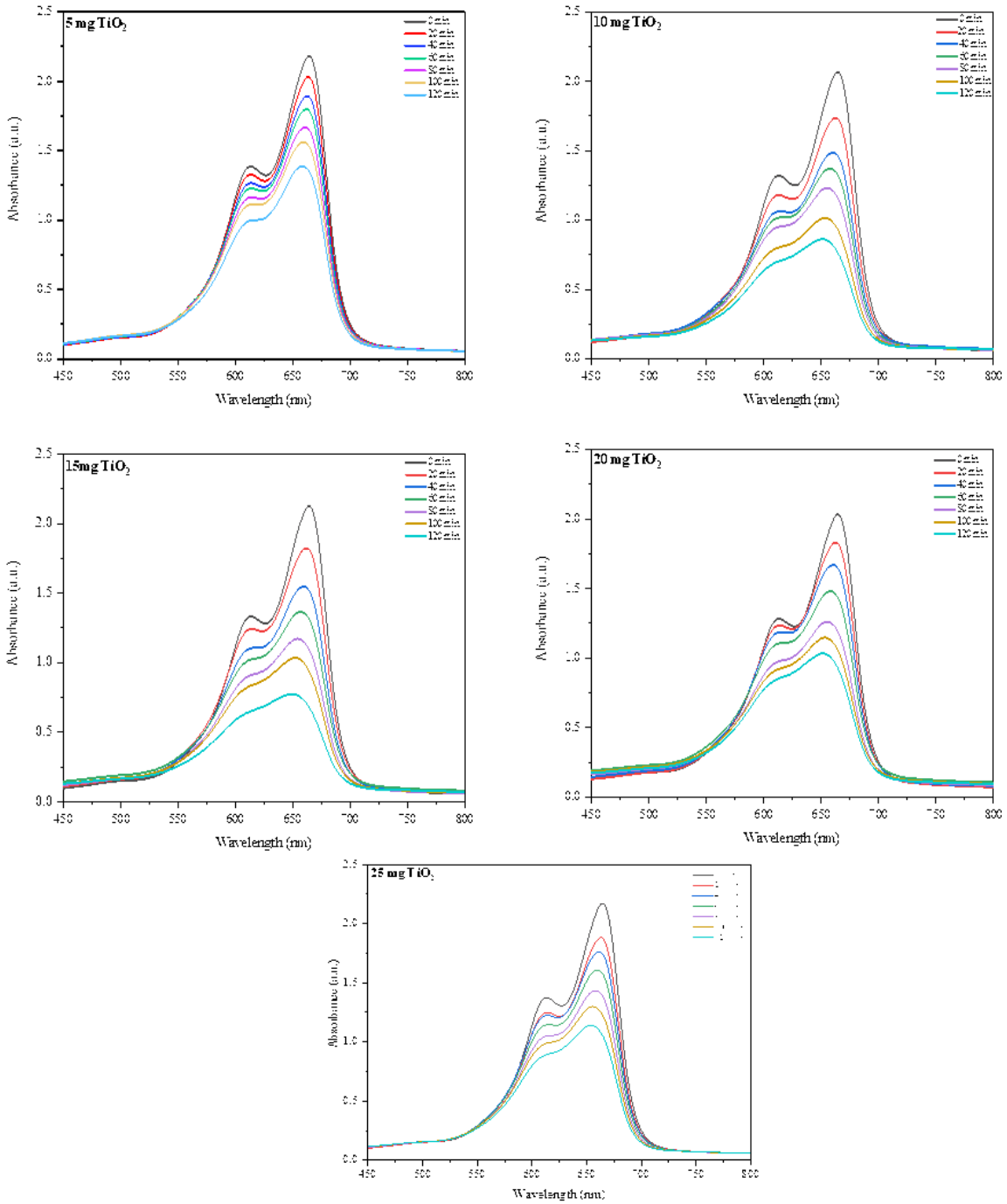

Figure 9. UV-Vis absorption spectra of TiO_2 samples after photocatalysis of MB solutions.

4. Conclusion

TiO_2 nanoparticles were prepared at room temperature using a sol-gel method with ethanol as a solvent and TTIP as the precursor. The XRD technique indicated that the average crystallite size of the prepared TiO_2 nanoparticles was 32.38 nm and 37.37 nm for anatase and rutile phases, respectively. Through XPS, the surface components are revealed, which are Ti 2p and O 1s regions. The FESEM and TEM images show that the material has agglomerated to produce spherical shapes. The BET surface area and pore width of the TiO_2 nanosphere are 33.36 m^2g^{-1} and 11 nm respectively. The results of the degradation process of MB using different doses of TiO_2 photocatalyst showed that the weight (15 mg) of the catalyst was the best dose for degrading MB dye and reached approximately 68.39% within 120 minutes.

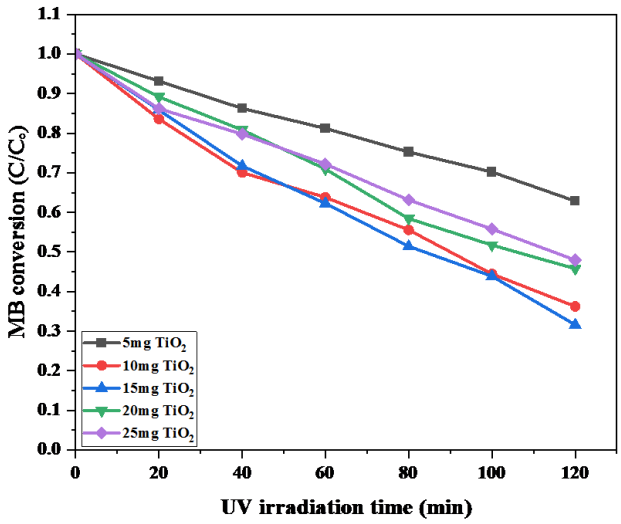

Figure 10. TiO_2 photocatalytic absorption performance under UV light.

Ethical approval
This manuscript does not report on or involve the use of any animal or human data or tissue. So the ethical approval is not applicable.

Authors Contributions
All the authors have participated sufficiently in the intellectual content, conception and design of this work or the analysis and interpretation of the data (when applicable), as well as the writing of the manuscript.

Availability of data and materials
The datasets generated and analyzed during the current study are available from the corresponding author upon reasonable request.

Conflict of Interests
The author declare that they have no known competing financial interests or personal relationships that could have appeared to influence the work reported in this paper.

References

[1] F. K. M. Alosfur, A. A. Ouda, N. J. Ridha, and S. H. Abud. "Structure and optical properties of TiO_2 nanorods prepared using polyol solvothermal method.". *AIP Conf. Proc.*, **2144**:030025, 2019.

[2] S. Padikkaparambil, B. Narayanan, Z. Yaakob, S. Viswanathan, and S. M. Tasirin. "Au/TiO_2 reusable photocatalysts for dye degradation.". *Int. J. Photoenergy*, **2013**:10, 2013.

[3] O. Alfano, D. Bahnemann, A. Cassano, R. Dillert, and R. Goslich. "Photocatalysis in water environments using artificial and solar light. ". *Catal. Today*, **58**: 199–230, 2000.

[4] M. H. H. Jumali, F. K. M. Alosfur, S. Radiman, N. J. Ridha, M. A. Yarmo, and A. A. Umar. "Rapid synthesis of TiO_2/MWCNTs nanocatalyst with enhanced photocatalytic activity using modified microwave technique.". *Mater. Sci. Semicond. Process.*, **25**:207–210, 2014.

[5] D. Wang, R. Yu, Y. Chen, N. Kumada, N. Kinomura, and M. Takano. "Photocatalysis property of needle-like TiO_2 prepared from a novel titanium glycolate precursor.". *Solid State Ion.*, **172**:101–104, 2004.

[6] F. Alosfur, M. H. Jumali, S. Radiman, N. J. Ridha, M. A. Yarmo, and A. A. Umar. "Visible light-responsive TiO_2 coated MWCNTs as a hybrid nanocatalysts.". *Int. J. Electrochem. Sci.*, **8**:2977–2982, 2013.

[7] M. H. Haji Jumali, K. M. A. A. Firas, S. Radiman, and A. A. Umar. "Dressing of MWCNTs with TiO_2 nanoparticles using modified microwave method.". *Adv. Mat. Res.*, **364**:228–231, 2012.

[8] S. Bao, K. Li, P. Ning, J. Peng, X. Jin, and L. Tang. "Highly effective removal of mercury and lead ions from wastewater by mercaptoamine-functionalized silica-coated magnetic nano-adsorbents: behaviours and mechanisms. ". *Appl. Surf. Sci.*, **393**:457–466, 2017.

[9] Y. Xu, W. Wen, M.-Z. Tang, and J.-M. Wu. "Photocatalytically active TiO_2 microtubes assembled with radially aligned nanowires. ". *Mater. Chem. Front.*, **1**: 1453–1458, 2017.

[10] J. Du, X. Lai, N. Yang, J. Zhai, D. Kisailus, F. Su, D. Wang, and L. Jiang. "Hierarchically ordered macro-mesoporous TiO_2-graphene composite films: improved mass transfer, reduced charge recombination, and their enhanced photocatalytic activities.". *ACS Nano.*, **5**:590–596, 2011.

[11] B. A. Jabar, H. M. Yaseen M. A. Hamzah, K. J. Tahir, N. J. Ridha, F. K. Mohamad Alosfur, R. A. Madlol, and B. M. Hussein. "Synthesis and structural properties of Eu^{3+}:TiO_2 nanoparticles. ". *J. Nanostruct.*, **11**: 136–142, 2021.

[12] M. Pelaez, N. T. Nolan, S. C. Pillai, M. K. Seery, P. Falaras, A. G. Kontos, P. S. Dunlop, J. W. Hamilton, J. A. Byrne, and K. O'shea. "A review on the visible light active titanium dioxide photocatalysts for environmental applications. ". *Appl. Catal. B*, **125**: 331–349, 2012.

[13] M. Fathy and H. Hamad. "Influence of calcination temperatures on the formation of anatase TiO_2 nano rods with a polyol-mediated solvothermal method.". *RSC Adv.*, **6**:7310–7316, 2016.

[14] N. J. Ridha, F. K. M. Alosfur, M. H. H. Jumali, and S. Radiman. "Effect of Al thickness on the structural and ethanol vapor sensing performance of ZnO porous nanostructures prepared by microwave-assisted hydrothermal method.". *J. Nanotechnol.*, **31**:145502, 2020.

[15] S. K. Pradhan, P. J. Reucroft, F. Yang, and A. Dozier. "Growth of TiO_2 nanorods by metalorganic chemical vapor deposition. ". *J. Cryst. Growth*, **256**:83–88, 2003.

[16] R. S. Jalawkhan, A. A. Ouda, A. M. Abdul-lettif, and F. K. M. Alosfur. "Effect of solvents on the morphology of TiO_2 nanoparticles prepared by microwave method.". *IOP Conf. Ser.: Mater. Sci. Eng.*, **928**: 072159, 2020.

[17] B. Ding, C. K. Kim, H. Y. Kim, M. K. Seo, and S. J. Park. "Titanium dioxide nanofibers prepared by using electrospinning method.". *Fibers Polym.*, **5**:105–109, 2004.

[18] F. Z. Haque, R. Nandanwar, and P. Singh. "Evaluating photodegradation properties of anatase and rutile TiO_2 nanoparticles for organic compounds. ". *Optik*, **128**: 191–200, 2017.

[19] P. Pookmanee and S. Phanichphant. "Titanium dioxide powder prepared by a sol-gel method. ". *J. Ceram. Process. Res.*, **10**:167–170, 2009.

[20] D. Bokov, A. Turki Jalil, S. Chupradit, W. Suksatan, M. Javed Ansari, I. H. Shewael, G. H. Valiev, and E. Kianfar. "Nanomaterial by sol-gel method: synthesis and application.". *Adv. Mater. Sci. Eng.*, **2021**: 1–21, 2021.

[21] C. Su, B.-Y. Hong, and C.-M. Tseng. "Sol–gel preparation and photocatalysis of titanium dioxide.". *Catal. Today*, **96**:119–126., 2004.

[22] Y. Li, M. Guo, M. Zhang, and X. Wang. "Hydrothermal synthesis and characterization of TiO_2 nanorod arrays on glass substrates. ". *Mater. Res. Bull.*, **44**: 1232–1237, 2009.

[23] H. Feng, L. Chen, L. Yuan, and Q. Cai. "Visible light-induced efficiently oxidative decomposition of p-Nitrophenol by CdTe/TiO_2 nanotube arrays.". , *J. Chem. Eng.*, **215**:591–599, 2013.

[24] X. Feng, X. Huang, and X. Wang. "Thermal conductivity and secondary porosity of single anatase TiO_2 nanowire. ". *J. Nanotechnol.*, **23**:185701, 2012.

[25] N. Wu, J. Wang, D. N. Tafen, H. Wang, J.-G. Zheng, J. P. Lewis, X. Liu, S. S. Leonard, and A. Manivannan. "Shape-enhanced photocatalytic activity of single-crystalline anatase TiO_2 (101) nanobelts.". *J. Am. Chem. Soc.*, **132**:6679–6685, 2010.

[26] M. Zhang, Q. Shang, Y. Wan, Q. Cheng, G. Liao, and Z. Pan. "Self-template synthesis of double-shell TiO_2@ ZIF-8 hollow nanospheres via sonocrystallization with enhanced photocatalytic activities in hydrogen generation.". *Appl. Catal. B*, **241**:149–158, 2019.

[27] G. Huang, W. Ye, C. Lv, D. S. Butenko, C. Yang, G. Zhang, P. Lu, Y. Xu, S. Zhang, and H. Wang. "Hierarchical red phosphorus incorporated TiO_2 hollow sphere heterojunctions toward superior photocatalytic hydrogen production.". *J. Mater. Sci. Technol.*, **108**: 18–25, 2022.

[28] B. Réti, Z. Major, D. Szarka, T. Boldizsár, E. Horváth, A. Magrez, L. Forró, A. Dombi, and K. Hernádi. "Influence of TiO_2 phase composition on the photocatalytic activity of TiO_2/MWCNT composites prepared by combined sol–gel/hydrothermal method.". *J. Mol. Catal. A: Chem.*, **414**:140–147, 2016.

[29] A. Vorontsov, E. Kabachkov, I. Balikhin, E. Kurkin, V. Troitskii, and P. Smirniotis. "Correlation of surface area with photocatalytic activity of TiO_2.". *J. Adv. Oxid. Technol*, **21**:127–137, 2018.

[30] G. Cernuto, N. Masciocchi, A. Cervellino, G. M. Colonna, and A. Guagliardi. "Size and shape dependence of the photocatalytic activity of TiO_2 nanocrystals: a total scattering Debye function study.". *J. Am. Chem. Soc.*, **133**:3114–3119, 2011.

[31] M. Salehi, H. Hashemipour, and M. Mirzaee. "Experimental study of influencing factors and kinetics in catalytic removal of methylene blue with TiO_2 nanopowder.". *Am J. Environ. Eng. ASCE*, **2**:1–7, 2012.

[32] A. Obaid and L. Ahmed. "One-step hydrothermal synthesis of α-MoO_3 nano-belts with ultrasonic assist for incorporating TiO_2 as a nanocomposite.". *Egypt J. Chem.*, **64**:5725–5734, 2021.

[33] M. Khalil, E. S. Anggraeni, T. A. Ivandini, and E. Budianto. "Exposing TiO_2 (001) crystal facet in nano Au-TiO_2 heterostructures for enhanced photodegradation of methylene blue. ". *Appl. Surf. Sci.*, **487**: 1376–1384, 2019.

[34] A. O. Juma, I. O. Acik, V. Mikli, A. Mere, and M. Krunks. "Effect of solution composition on anatase to rutile transformation of sprayed TiO_2 thin films.". *Thin Solid Films*, **594**:287–292, 2015.

[35] O. S. N. Ghosh, S. R. Allam, S. Gayathri, G. Chakravarthy, A. Sharan, and A. K. Viswanath. "Direct evidence for the increase in exciton concentration and effective electron-hole pair separation in anatase TiO_2: Eu nanospheres by using femtosecond Z-scan.". *The National Laser Symposium (NLS-24), India*, , 2015.

[36] D. Fang, F. He, J. Xie, and L. Xue. "Calibration of binding energy positions with C 1s for XPS results.". *J. Wuhan Univ. Technol. Mater. Sci. Ed.*, **35**:711–718, 2020.

[37] R. T. Konatu, D. D. Domingues, R. França, and A. P. R. Alves. "XPS characterization of TiO_2 nanotubes growth on the surface of the Ti15Zr15Mo alloy for biomedical applications.". *J. Funct. Biomater.*, **14**:353, 2023.

[38] X. Wang, Q. Xiang, B. Liu, L. Wang, T. Luo, D. Chen, and G. Shen. " TiO_2 modified FeS nanostructures with enhanced electrochemical performance for lithium-ion batteries ". *Sci. Rep.*, **3**:2007, 2013.

[39] L. Armelao, D. Barreca, G. Bottaro, A. Bovo, A. Gasparotto, and E. Tondello. "Characterization of Au/TiO_2 nanocomposites by XPS. ". *Surf. Sci. Spectra*, **10**:1–7, 2003.

[40] Nasikhudin, M. Diantoro, A. Kusumaatmaja, and K. Triyana. "Study on Photocatalytic Properties of TiO_2 Nanoparticle in various pH condition.". *J. Phys. Conf. Ser.*, **1011**:012069, 2018.

[41] S. B. Somwanshi, S. B. Somvanshi, and P. B. Kharat. "Visible light driven photocatalytic activity of TiO_2 nanoparticles prepared via gel-combustion process.". *J. Phys. Conf. Ser.*, **1644**:012042, 2020.

[42] K. Sing, D. Everett, R. Haul, L. Moscou, R. Pierotti, J. Rouquerol, and T. Siemieniewska. "Annexes: IUPAC recommendations: reporting physisorption data for gas/solid systems.". *Handb. Heterog. Catal.*, **3**: 1503–1516, 2008.

[43] K. Kinashi, Y. Kambe, M. Misaki, Y. Koshiba, K. Ishida, and Y. Ueda. "Synthesis, characterization, photo-induced alignment, and surface orientation of poly (9, 9-dioctylfluorene-alt-azobenzene)s. ". *Journal of Polymer Science Part A: Polymer Chemistry*, **50**:5107–5114, 2012.

[44] M. Thommes, K. Kaneko, A. V. Neimark, J. P. Olivier, F. Rodriguez-Reinoso, J. Rouquerol, and K. S. Sing. "Physisorption of gases, with special reference to the evaluation of surface area and pore size distribution (IUPAC Technical Report).". *Pure Appl. Chem.*, **87**: 1051–1069, 2015.

[45] M. U. Farooq, X. Zhang, Y. Guan, W. Chen, J. Zhou, J. Zhang, G. Qian, X. Duan, X. Zhou, and W. Yuan. "Synergistic electronic and geometric effects of Au/CeO_2 catalyst for oxidative esterification of methacrolein.". *AIChE J.*, **69**:e17932, 2023.

[46] F. K. Mohamad Alosfur, N. J. Ridha, M. H. H. Jumali, and S. Radiman. "One-step formation of TiO_2 hollow spheres via a facile microwave-assisted process for photocatalytic activity.". *Nanotechnology*, **29**:145707, 2018.

[47] F. K. M. Alosfur, N. J. Ridha, M. H. H. Jumali, and S. Radiman. "One-step formation of TiO_2 hollow spheres via a facile microwave-assisted process for photocatalytic activity.". *Nanotechnology*, **29**:145707, 2018.